Mathematical and Computational Applications

MDPI

Article

Analytical Solutions of PBTK Models for Evaluating the Impact of Surface Diffusion Characteristics on the Leaching Profile of Implant Byproducts

Matheos Giakoumi [1,2,3], Konstantinos Kapnisis [1], Andreas Anayiotos [1] and Pavlos S. Stephanou [4,*]

[1] Department of Mechanical Engineering and Materials Science and Engineering, Cyprus University of Technology, Limassol 3036, Cyprus; matheos.giakoumi@utexas.edu (M.G.); k.kapnisis@cut.ac.cy (K.K.); andreas.anayiotos@cut.ac.cy (A.A.)
[2] Fondazione Eni Enrico Mattei, Corso Magenta 63, 20123 Milan, Italy
[3] Hildebrand Department of Petroleum and Geosystems Engineering, The University of Texas at Austin, Austin, TX 78712, USA
[4] Department of Chemical Engineering, Cyprus University of Technology, 30 Archbishop Kyprianou Str., Limassol 3036, Cyprus
* Correspondence: pavlos.stefanou@cut.ac.cy

Abstract: Toxicokinetic or pharmacokinetic models, physiologically based or not, offer a unique avenue to understand the transport of toxins or pharmaceuticals in living organisms. The availability of analytical solutions to such models offers the means to engage in a plethora of applications. In the present work, we provide the framework to solve analytically such models using the matrix exponential, and we then apply this method to derive an explicit solution to four-to-five-compartment physiologically based toxicokinetic (PBTK) models considering a single- and an infinite-exponential expression for the amount of mass released from an implantable device. We also offer the conditions that need to be met for analytical solutions to be obtained when the kinetic rates are time-dependent functions. Our analysis compares the computation time between analytical and numerical solutions and characterizes the dependency of the maximum substance mass value and the time it occurs in the various tissue compartments from the material surface diffusion characteristics. Our analytical solutions, which have several advantages over the solutions obtained using numerical solvers, can be incorporated into *in silico* tools and provide valuable information for human health risk assessment.

Keywords: medical implants; physiologically based toxicokinetic (PBTK) models; modeling and simulations (M&S); absorption, distribution, metabolism, and excretion (ADME); analytical solutions; matrix exponential

check for updates

Citation: Giakoumi, M.; Kapnisis, K.; Anayiotos, A.; Stephanou, P.S. Analytical Solutions of PBTK Models for Evaluating the Impact of Surface Diffusion Characteristics on the Leaching Profile of Implant Byproducts. *Math. Comput. Appl.* **2024**, *29*, 101. https://doi.org/10.3390/mca29060101

Academic Editor: Alexandre Souto Martinez

Received: 12 September 2024
Revised: 26 October 2024
Accepted: 28 October 2024
Published: 4 November 2024

Copyright: © 2024 by the authors. Licensee MDPI, Basel, Switzerland. This article is an open access article distributed under the terms and conditions of the Creative Commons Attribution (CC BY) license (https://creativecommons.org/licenses/by/4.0/).

1. Introduction

Understanding and modeling the kinetics of substances (toxins or pharmaceuticals) in living organisms is vital. It allows us to provide a framework for health risk assessment and management [1–4] and for the *in silico* optimization of novel drug delivery systems [5,6]. Indeed, recently, the US Food and Drug Administration (FDA) [7] and the European Centre for Disease Prevention and Control (ECDC) [8] suggested that modeling and simulation tools are valuable and should be employed to assist decision-making. Such *in silico* tools, therefore, allow the reduction of animals sacrificed for testing, reduction of the cost and time for performing such testing, and improving the toxicity prediction and safety assessment [9].

In such an endeavor, mathematical models have a unique position; mathematical modeling enables us to comprehend the underlying mechanics of various processes and even to explore scenarios that would have otherwise been impossible or too difficult to study experimentally. As such, it bears today, given the advent of computational power, a

pivotal role not only in developing toxicokinetic or pharmacokinetic models but practically in our everyday lives.

An important class of mathematical models is physiologically based toxicokinetic (PBTK) [1,10] and physiologically based pharmacokinetic (PBPK) models [11]. Both PBTK and PBPK models quantitatively describe the absorption, distribution, metabolism, and excretion (ADME) of substances (either toxic in PBTK models or drugs in PBPK models) [10]. In essence, they are mass balances that describe how the mass of the substance(s) diffuses throughout the body by focusing on a set of compartments (e.g., body organs, biofluids, and tissues) characterized physiologically using a system of coupled ordinary differential equations (ODEs) [10]. The kinetic rates quantify the transport of the substance from one compartment to another, and each describes, in a single parameter, the multitude of biological and physicochemical processes that occur during mass transfer from one compartment to another [10]. For example, Saylor et al. [12] are perhaps the first to provide a biokinetic model to estimate nickel release from an implanted device. The Saylor et al. model (SM) aims to describe the transfer of Ni ions from the implanted medical device to adjacent tissue and circulation and their transport between blood and the various tissues/organs by combining a traditional toxicokinetic compartmental model with a physics-based model. Saylor et al. used this model to predict local and systemic nickel exposure from nitinol devices produced using a wide range of manufacturing processes. In our recent work [2], we formulated the SMK model by adding one additional compartment corresponding to kidneys. The separate consideration of kidneys from the "other tissues" compartment makes the new SMK model a better approximation of the physiological secretion of nickel through the urinary system. Both models were noted to provide similar comparisons with human clinical data; however, when the two models are compared against the *in vivo* minipig data of Nagaraja et al. [13], the SMK model is more accurate in predicting the concentration–time profile in the urine compartment (see Figures 4 and S2–S4 of Giakoumi et al. [2]). More recently, we have presented a multi-compartmental PBTK model that includes as separate compartments many important tissues and organs (e.g., liver, lungs, and brain), body fluids, and excreta, which has demonstrated prognostic conformity with in-house *in vivo* mice data [3].

Although recent work has emphasized the need to include a multitude of simulation tools to address the full capacity of PBTK and PBPK models, including the use of multi-objective optimization and stochastic Monte Carlo simulations to accommodate a more precise and trustworthy assessment [2,3], the complexity of said tools does not allow analytical solutions to be sought. To the best of our knowledge, only the work of Abuhelwa et al. [14] has reported analytical solutions for PBPK models using the Laplace transform method. In this work, we aim to fill this void by providing analytical solutions to PBTK models with four to five compartments that monitor the biodistribution of substance leaching from medical device materials. Providing solutions to multi-compartment PBTK (or PBPK) models with more than five compartments that better reflect human anatomy and physiology is a straightforward exercise. To do this, we use the fact that the analytical solution of any linear system of coupled ODEs involves the matrix exponential. We explicitly derive, as illustrated in the next section, the matrix exponential for the two PBTK models of interest (SM and SMK) and provide the explicit solution for both models, which, to the best of our knowledge, has not been published before.

The structure of the paper is as follows: in the next section, we provide the well-known general solution to any linear system of coupled ODEs that involves the matrix exponential [15]. The two previously published PBTK models are studied considering a single- and an infinite-exponential device release with time-independent kinetic rates (the former provided in the Supplementary Material). A note regarding obtaining an analytical solution when the kinetic rates are arbitrary functions of time is also provided. In Section 3, we first compare the computation time between analytical and numerical solutions and provide the concentration–time profiles for some parameter values. We then, and most importantly, examine the model-derived predictions to characterize the dependency of the

maximum substance mass value and the time it occurs in the various tissue compartments from the device material surface finishing. We end with Section 4 where we summarize the most important results of this study.

2. Methods

Any linear system of ODEs can be written in the following tensorial form:

$$\frac{d\mathbf{y}(t)}{dt} = \mathbf{A} \cdot \mathbf{y}(t) + \mathbf{b}(t), \tag{1}$$

where $\mathbf{y}(t)$ is the vector of dependent variables, such that $\mathbf{y}(t = 0) = 0$. Note that, in general, the non-homogenous part of the system of coupled ODEs is an arbitrary function of time. The well-known solution then comes easily by applying the Laplace transform [15]:

$$s\mathbf{Y}(s) = \mathbf{A} \cdot \mathbf{Y}(s) + \mathbf{B}(s) \Rightarrow \mathbf{Y}(s) = (s\mathbf{I} - \mathbf{A})^{-1} \cdot \mathbf{B}(s), \tag{2}$$

where $\mathbf{I}$ is the unit tensor. Then, by inversing the Laplace transform, we obtain [15]:

$$\mathbf{y}(t) = \int_0^t e^{\mathbf{A}(t-x)} \cdot \mathbf{b}(x)dx, \tag{3}$$

where $e^{\mathbf{A}t}$ is the matrix exponential of $\mathbf{A}t$ [15,16]. One way to obtain the matrix exponential is to use Sylvester's formula (or the Lagrange interpolating polynomial method) [16], which necessitates first finding the eigenvalues and eigenvectors of $\mathbf{A}$. We will now illustrate this method in specific examples regarding solving two PBTK models.

2.1. The Saylor et al. Model

The SM model [12] was the first model proposed to predict the biodistribution of nickel release from an implanted medical device. It considers a zero-order rate of absorption of dietary nickel from the gut into serum (k_g), a first-order elimination of Ni from the serum through urine (k_u), a first-order elimination of Ni from the local tissues through serum (k_l), and a first-order exchange of Ni between serum and tissues (k_{st} and k_{ts}). This model's predictive capacity has been previously validated against reported values following implantation of atrium occluders in humans [17] and stent implantation in minipigs [13] by Giakoumi et al. [2]. It reads as follows,

$$\begin{array}{l} \frac{dM_l(t)}{dt} = (1 - F(t))\dot{M}_d(t) - k_l(t)M_l(t) \\ \frac{dM_s(t)}{dt} = F(t)\dot{M}_d(t) - (k_{st} + k_u)M_s(t) + k_l M_l(t) + k_{ts}M_t(t) + k_g \\ \frac{dM_t(t)}{dt} = k_{st}M_s(t) - k_{ts}M_t(t) \end{array}, \tag{4a}$$

where M_l, M_s, M_t correspond to the mass of nickel in the local tissue, serum, and other tissue compartments, respectively. In addition, the urine mass is given via a first-order elimination equation:

$$\frac{dM_u(t)}{dt} = C_u(t)Q_u = k_u M_s(t), \tag{4b}$$

where C_u corresponds to the concentration of nickel in urine, and Q_u corresponds to the volumetric urine output rate. Note that C_u is simply proportional to $M_s(t)$; similarly, the nickel concentration in serum is given as $C_s(t) = M_s(t)/V_s$ where V_s corresponds to the serum volume. Also, $\dot{M}_d(t) \equiv dM_d/dt$ represents the nickel release generated from the medical device, of which only a fraction ($0 \leq F \leq 1$) is released directly into the serum, while the remaining nickel partitions into the local tissue surrounding the device. Note that this fraction and the kinetic rate k_l are non-negative and, in general, time-dependent [2]; however, we will herein consider them to be constants for simplicity unless otherwise

specified (see also Section 2.3). The initial (control) conditions at $t = 0$ for these quantities (that also stand as their steady-state values) are the following:

$$M_l(0) = 0, M_s(0) = \frac{k_g}{k_u}, M_t(0) = \frac{k_{st}}{k_{ts}} M_s(0). \tag{4c}$$

Now, the analytical solution of the first equation in Equation (4a) is trivial and can easily be provided as:

$$\begin{array}{l} M_l(t) = \exp[-\theta(t)] \int\limits_0^t \exp[\theta(x)](1 - F(x))\dot{M}_d(x)dx \\ \theta(t) = \int\limits_0^t k_l(x)dx \end{array}. \tag{5}$$

Thus, since $M_l(t)$ is known, then the system of remaining ODEs in Equation (4a) is written as:

$$\begin{array}{l} \frac{dM_s(t)}{dt} = F(t)\dot{M}_d(t) - (k_{st} + k_u)M_s(t) + k_l M_l(t) + k_{ts} M_t(t) + k_g \\ \frac{dM_t(t)}{dt} = k_{st} M_s(t) - k_{ts} M_t(t) \end{array}, \tag{6}$$

This can then be written in the form of Equation (1) using:

$$\mathbf{y}(t) = \begin{bmatrix} M_s(t) - M_s(0) \\ M_t(t) - M_t(0) \end{bmatrix}, \mathbf{A} = \begin{bmatrix} -(k_{st} + k_u) & k_{ts} \\ k_{st} & -k_{ts} \end{bmatrix}, \mathbf{b}(t) = g(t) \begin{bmatrix} 1 \\ 0 \end{bmatrix}, \tag{7a}$$

where

$$g(t) = F(t)\dot{M}_d(t) + k_l(t)M_l(t). \tag{7b}$$

We next need to obtain the matrix exponential. First, we must obtain the eigenvalues of $\mathbf{A}$,

$$\begin{array}{l} \det(\mathbf{A} - \lambda \mathbf{I}) = \lambda^2 - \mathrm{tr}\mathbf{A}\lambda + \det\mathbf{A} = 0 \Rightarrow \\ \lambda^2 + (k_{st} + k_u + k_{ts})\lambda + k_u k_{ts} = 0 \end{array}. \tag{8}$$

Given that the discriminant of this equation is:

$$\begin{array}{l} \Delta = (\mathrm{tr}\mathbf{A})^2 - 4\det\mathbf{A} = (k_{st} + k_u + k_{ts})^2 - 4k_u k_{ts} \\ = k_{ts}^2 + k_{st}^2 + k_u^2 + 2k_{st}k_{ts} + 2k_u(k_{st} - k_{ts}) \end{array}, \tag{9}$$

and since the kinetic rates are non-negative, the eigenvalues of $\mathbf{A}$ are always real (i.e., $\Delta > 0$) provided that $k_{st} > k_{ts}$. Note, however, that this condition may be too restrictive since any other choice of parameter values may still provide real eigenvalues even if $k_{st} < k_{ts}$ as long as $\Delta > 0$. Then, the eigenvalues of $\mathbf{A}$ are:

$$\lambda_{1,2} = \frac{1}{2}\left(\mathrm{tr}\mathbf{A} \pm \sqrt{\Delta}\right) = -\frac{1}{2}\left[(k_{st} + k_u + k_{ts}) \mp \sqrt{\Delta}\right]. \tag{10}$$

For the system to be dynamically stable, we need to have all eigenvalues with a negative real part. Thus, it should hold

$$\mathrm{tr}\mathbf{A} < \sqrt{\Delta} \Rightarrow (\mathrm{tr}\mathbf{A})^2 < \Delta \Rightarrow \det\mathbf{A} = k_u k_{ts} > 0. \tag{11}$$

Since the kinetic rates are non-negative, then this automatically holds. Then, by using Sylvester's formula:

$$\begin{array}{l} e^{\mathbf{A}t} = \frac{\mathbf{A} - \lambda_2 \mathbf{I}}{\lambda_1 - \lambda_2} e^{\lambda_1 t} + \frac{\mathbf{A} - \lambda_1 \mathbf{I}}{\lambda_2 - \lambda_1} e^{\lambda_2 t} = P_1(t)\mathbf{A} + P_0(t)\mathbf{I} \\ P_1(t) = \frac{e^{\lambda_1 t} - e^{\lambda_2 t}}{\lambda_1 - \lambda_2}, P_0(t) = -\frac{\lambda_2 e^{\lambda_1 t} - \lambda_1 e^{\lambda_2 t}}{\lambda_1 - \lambda_2} \end{array}. \tag{12}$$

Thus,

$$\begin{array}{l} \int_0^t e^{\mathbf{A}(t-x)} \cdot \mathbf{b}(x)dx = \begin{bmatrix} -(k_{st}+k_u) \\ k_{st} \end{bmatrix} I_1(t) + \begin{bmatrix} 1 \\ 0 \end{bmatrix} I_0(t), \\ I_i(t) = \int_0^t P_i(t-x)g(x)dx \end{array} . \quad (13)$$

Finally,

$$\begin{array}{l} M_s(t) - M_s(0) = -(k_{st}+k_u)I_1(t) + I_0(t) \\ M_t(t) - M_t(0) = k_{st}I_1(t) \end{array} . \quad (14)$$

These expressions are general in that they apply to any device release expression.

We will now specify the device release to be equal to the one we have suggested recently [2]:

$$M_d(t) = A_{\text{surf}}a\left[1 - \sum_{n=1,odd}^{\infty} \frac{8}{(\pi n)^2} \exp\left(-\frac{n^2 t}{\tau}\right)\right]. \quad (15)$$

where A_{surf} is the surface area, a is the amount of surface-connected nickel per surface area, and τ is a characteristic release time. A simplified single-exponential expression, as was used by various researchers [12,18,19] (without a Higuchi-type dissolution kinetics [20]), can also be employed; the results obtained in this case can be found in the Supplementary Material.

Then, the solution for the local tissue when F and k_l are time-independent is given via Equation (5) and equals to,

$$M_l(t) = (1-F)A_{\text{surf}}a \sum_{n=1,odd}^{\infty} \frac{8}{\pi^2} \frac{1}{k_l\tau - n^2}\left[\exp\left(-\frac{n^2 t}{\tau}\right) - \exp(-k_l t)\right]. \quad (16)$$

Finally, the definitions for the functions $I_i(t)$ need to be defined as

$$\begin{array}{l} I_0(t) = -A_{\text{surf}}a\left\{\frac{F}{\lambda_1-\lambda_2}\frac{8}{\pi^2\tau}\sum_{n=1,odd}^{\infty}\left[\lambda_2 A_1^n(t) - \lambda_1 A_2^n(t)\right] + \right. \\ \left. \frac{(1-F)k_l}{\lambda_1-\lambda_2}\left[\left\{\sum_{n=1,odd}^{\infty}\frac{8}{\pi^2}\frac{\lambda_2 A_1^n(t) - \lambda_1 A_2^n(t)}{k_l\tau - n^2}\right\} - \left(\sum_{n=1,odd}^{\infty}\frac{8}{\pi^2}\frac{1}{k_l\tau-n^2}\right)\left[\lambda_2 B_1(t) - \lambda_1 B_2(t)\right]\right]\right\} \\ I_1(t) = A_{\text{surf}}a\left\{\frac{F}{\lambda_1-\lambda_2}\frac{8}{\pi^2\tau}\sum_{n=1,odd}^{\infty}\left[A_1^n(t) - A_2^n(t)\right] + \right. \\ \left. \frac{(1-F)k_l}{\lambda_1-\lambda_2}\left[\left\{\sum_{n=1,odd}^{\infty}\frac{8}{\pi^2}\frac{A_1^n(t) - A_2^n(t)}{k_l\tau - n^2}\right\} - \left(\sum_{n=1,odd}^{\infty}\frac{8}{\pi^2}\frac{1}{k_l\tau-n^2}\right)\left[B_1(t) - B_2(t)\right]\right]\right\} \end{array} , \quad (17a)$$

where

$$\begin{array}{l} A_i^n(t) = \int_0^t e^{\lambda_i(t-x)}\exp\left(-\frac{n^2 x}{\tau}\right)dx = \frac{\tau}{\lambda_i\tau + n^2}\left[\exp(\lambda_i t) - \exp\left(-\frac{n^2 t}{\tau}\right)\right] \\ B_i(t) = \int_0^t e^{\lambda_i(t-x)}\exp(-k_l x)dx = \frac{\tau}{\lambda_i\tau + k_l\tau}\left[\exp(\lambda_i t) - \exp(-k_l t)\right] \end{array} , \quad (17b)$$

2.2. The SMK Model

The SMK model reads as follows [2],

$$\begin{array}{l} \frac{dM_l(t)}{dt} = (1-F(t))\dot{M}_d(t) - k_l(t)M_l(t) \\ \frac{dM_s(t)}{dt} = F(t)\dot{M}_d(t) - (k_{st}+k_{sk})M_s(t) + k_l M_l(t) + k_{ks}M_k(t) + k_{ts}M_t(t) + k_g \\ \frac{dM_t(t)}{dt} = k_{st}M_s(t) - k_{ts}M_t(t) \\ \frac{dM_k(t)}{dt} = k_{sk}M_s(t) - (k_{ks}+k_u)M_k(t) \\ \frac{dM_u(t)}{dt} = C_u(t)Q_u = k_u M_k(t) \end{array} , \quad (18a)$$

where M_k corresponds to the mass of nickel in the kidneys compartment for which a first-order exchange of Ni between serum and kidneys (k_{sk} and k_{ks}) is considered. The

SMK model's predictive capacity has been previously validated against reported values following stent implantation in minipigs [13] by Giakoumi et al. [2].

The initial (control) conditions at $t = 0$ for these quantities are the following:

$$M_l(0) = 0, M_s(0) = \frac{k_g}{k_{sk}} \frac{k_{ks} + k_u}{k_u}, M_t(0) = \frac{k_{st}}{k_{ts}} M_s(0), M_k(0) = \frac{k_{sk}}{k_{ks} + k_u} M_s(0). \quad (18b)$$

The solution to the first equation is again Equation (5) so that the system comprising the 2nd to 4th ODEs in Equation (18a) can be written in the form of Equation (1) where

$$\mathbf{y}(t) = \begin{bmatrix} M_s(t) - M_s(0) \\ M_t(t) - M_t(0) \\ M_k(t) - M_k(0) \end{bmatrix}, \mathbf{A} = \begin{bmatrix} -(k_{sk} + k_{st}) & k_{ts} & k_{ks} \\ k_{st} & -k_{ts} & 0 \\ k_{sk} & 0 & -(k_{ks} + k_u) \end{bmatrix}, \mathbf{b}(t) = g(t) \begin{bmatrix} 1 \\ 0 \\ 0 \end{bmatrix}. \quad (19)$$

and $g(t)$ is still given by Equation (7b). The eigenvalues of $\mathbf{A}$ are obtained from the characteristic equation:

$$\begin{array}{l} \det(\mathbf{A} - \lambda \mathbf{I}) = \lambda^3 + a_2\lambda^3 + a_1\lambda + a_0 = 0 \\ a_2 = -\mathrm{tr}\mathbf{A} = k_{ts} + k_{sk} + k_{st} + k_{ks} + k_u > 0 \\ a_1 = \frac{1}{2}\left[(\mathrm{tr}\mathbf{A})^2 - \mathrm{tr}\left(\mathbf{A}^2\right)\right] = (k_{ts} + k_{sk} + k_{st})(k_{ks} + k_u) > 0 \\ a_0 = -\det\mathbf{A} = (k_{sk}k_{ts} + k_{ks}k_{st})(k_{ks} + k_u) > 0 \end{array}. \quad (20)$$

Note that all coefficients of the polynomial are positive. Then, the Routh–Hurwitz stability criterion [15] necessitates that the roots of this polynomial are all with a negative real part when

$$\begin{array}{l} a_2a_1 - a_0 > 0 \Rightarrow \\ (k_{ts} + k_{sk} + k_{st} + k_{ks} + k_u)(k_{ts} + k_{sk} + k_{st})(k_{ks} + k_u) - (k_{sk}k_{ts} + k_{ks}k_{st})(k_{ks} + k_u) > 0 \Rightarrow \\ [(k_{ts} + k_{sk} + k_{st} + k_{ks} + k_u)(k_{ts} + k_{sk} + k_{st}) - (k_{sk}k_{ts} + k_{ks}k_{st})](k_{ks} + k_u) > 0 \Rightarrow \\ \left[(k_{ts} + k_{sk} + k_{st})^2 + k_u(k_{ts} + k_{sk} + k_{st}) + k_{ts}(k_{ks} - k_{sk})\right](k_{ks} + k_u) > 0 \end{array}. \quad (21)$$

Since all kinetic rates are non-negative, the Routh–Hurwitz stability criterion requires that $k_{ks} > k_{sk}$. Again, note that this requirement may be too restrictive since any other choice of the parameter values may still provide eigenvalues with a negative real part even if $k_{ks} < k_{sk}$ as long as $a_2a_1 - a_0 > 0$. Moreover, it is known that when the coefficients of a polynomial of any order are positive, then all of its roots have a negative real part [21]. Generally, the eigenvalues of $\mathbf{A}$ can be obtained and expressed in a closed form but are lengthy and will not be given here. Then, by using Sylvester's formula

$$\begin{array}{l} e^{\mathbf{A}t} = \frac{\mathbf{A}-\lambda_2\mathbf{I}}{\lambda_1-\lambda_2}\frac{\mathbf{A}-\lambda_3\mathbf{I}}{\lambda_1-\lambda_3}e^{\lambda_1 t} + \frac{\mathbf{A}-\lambda_1\mathbf{I}}{\lambda_2-\lambda_1}\frac{\mathbf{A}-\lambda_3\mathbf{I}}{\lambda_2-\lambda_3}e^{\lambda_2 t} + \frac{\mathbf{A}-\lambda_1\mathbf{I}}{\lambda_3-\lambda_1}\frac{\mathbf{A}-\lambda_2\mathbf{I}}{\lambda_3-\lambda_2}e^{\lambda_3 t} \\ = P_2(t)\mathbf{A}^2 + P_1(t)\mathbf{A} + P_0(t)\mathbf{I}, \\ P_2(t) = \frac{e^{\lambda_1 t}}{(\lambda_1-\lambda_2)(\lambda_1-\lambda_3)} + \frac{e^{\lambda_2 t}}{(\lambda_2-\lambda_1)(\lambda_2-\lambda_3)} + \frac{e^{\lambda_3 t}}{(\lambda_3-\lambda_1)(\lambda_3-\lambda_2)}, \\ P_1(t) = -\frac{(\lambda_2+\lambda_3)e^{\lambda_1 t}}{(\lambda_1-\lambda_2)(\lambda_1-\lambda_3)} - \frac{(\lambda_1+\lambda_3)e^{\lambda_2 t}}{(\lambda_2-\lambda_1)(\lambda_2-\lambda_3)} - \frac{(\lambda_1+\lambda_2)e^{\lambda_3 t}}{(\lambda_3-\lambda_1)(\lambda_3-\lambda_2)}, \\ P_0(t) = \frac{\lambda_2\lambda_3 e^{\lambda_1 t}}{(\lambda_1-\lambda_2)(\lambda_1-\lambda_3)} + \frac{\lambda_1\lambda_3 e^{\lambda_2 t}}{(\lambda_2-\lambda_1)(\lambda_2-\lambda_3)} + \frac{\lambda_1\lambda_2 e^{\lambda_3 t}}{(\lambda_3-\lambda_1)(\lambda_3-\lambda_2)}. \end{array} \quad (22)$$

Thus,

$$\begin{array}{l} \int_0^t e^{\mathbf{A}(t-x)} \cdot \mathbf{b}(x)dx = \begin{bmatrix} (k_{sk} + k_{st})^2 + k_{ts}k_{st} + k_{ks}k_{sk} \\ -k_{st}(k_{sk} + k_{st} + k_{ts}) \\ -k_{sk}(k_{sk} + k_{st} + k_{ks} + k_u) \end{bmatrix} I_2(t) + \begin{bmatrix} -(k_{sk} + k_{st}) \\ k_{st} \\ k_{sk} \end{bmatrix} I_1(t) + \begin{bmatrix} 1 \\ 0 \\ 0 \end{bmatrix} I_0(t) \\ I_i(t) = \int_0^t P_i(t-x)g(x)dx \end{array}. \quad (23)$$

Finally,

$$\begin{array}{l} M_s(t) - M_s(0) = \left[(k_{sk} + k_{st})^2 + k_{ts}k_{st} + k_{ks}k_{sk}\right] I_2(t) - (k_{sk} + k_{st}) I_1(t) + I_0(t) \\ M_t(t) - M_t(0) = -k_{st}(k_{sk} + k_{st} + k_{ts}) I_2(t) + k_{st} I_1(t) \\ M_k(t) - M_k(0) = -k_{sk}(k_{sk} + k_{st} + k_{ks} + k_u) I_2(t) + k_{sk} I_1(t) \end{array} . \quad (24)$$

When we consider an infinite-exponential device release, Equation (15), then the functions $I_i(t)$ need to be defined as

$$\begin{array}{l} I_0(t) = A_{\text{surf}} a \left\{ \dfrac{F}{\tau} \dfrac{8}{\pi^2} \displaystyle\sum_{n=1,odd}^{\infty} \left[\dfrac{\lambda_2\lambda_3 A_1^n(t)}{(\lambda_1-\lambda_2)(\lambda_1-\lambda_3)} + \dfrac{\lambda_1\lambda_3 A_2^n(t)}{(\lambda_2-\lambda_1)(\lambda_2-\lambda_3)} + \dfrac{\lambda_1\lambda_2 A_3^n(t)}{(\lambda_3-\lambda_1)(\lambda_3-\lambda_2)} \right] \right. \\ + (1-F) k_l \displaystyle\sum_{n=1,odd}^{\infty} \dfrac{8}{\pi^2} \dfrac{1}{k_l\tau - n^2} \left\{ \dfrac{\lambda_2\lambda_3 A_1^n(t)}{(\lambda_1-\lambda_2)(\lambda_1-\lambda_3)} + \dfrac{\lambda_1\lambda_3 A_2^n(t)}{(\lambda_2-\lambda_1)(\lambda_2-\lambda_3)} + \dfrac{\lambda_1\lambda_2 A_3^n(t)}{(\lambda_3-\lambda_1)(\lambda_3-\lambda_2)} \right\} \\ \left. - (1-F) k_l \left(\displaystyle\sum_{n=1,odd}^{\infty} \dfrac{8}{\pi^2} \dfrac{1}{k_l\tau - n^2} \right) \left[\dfrac{\lambda_2\lambda_3 B_1(t)}{(\lambda_1-\lambda_2)(\lambda_1-\lambda_3)} + \dfrac{\lambda_1\lambda_3 B_2(t)}{(\lambda_2-\lambda_1)(\lambda_2-\lambda_3)} + \dfrac{\lambda_1\lambda_2 B_3(t)}{(\lambda_3-\lambda_1)(\lambda_3-\lambda_2)} \right] \right) \\ I_1(t) = -A_{\text{surf}} a \left\{ \dfrac{F}{\tau} \dfrac{8}{\pi^2} \displaystyle\sum_{n=1,odd}^{\infty} \left[\dfrac{(\lambda_2+\lambda_3) A_1^n(t)}{(\lambda_1-\lambda_2)(\lambda_1-\lambda_3)} + \dfrac{(\lambda_1+\lambda_3) A_2^n(t)}{(\lambda_2-\lambda_1)(\lambda_2-\lambda_3)} + \dfrac{(\lambda_1+\lambda_2) A_3^n(t)}{(\lambda_3-\lambda_1)(\lambda_3-\lambda_2)} \right] \right. \\ + (1-F) k_l \displaystyle\sum_{n=1,odd}^{\infty} \dfrac{8}{\pi^2} \dfrac{1}{k_l\tau - n^2} \left\{ \dfrac{(\lambda_2+\lambda_3) A_1^n(t)}{(\lambda_1-\lambda_2)(\lambda_1-\lambda_3)} + \dfrac{(\lambda_1+\lambda_3) A_2^n(t)}{(\lambda_2-\lambda_1)(\lambda_2-\lambda_3)} + \dfrac{(\lambda_1+\lambda_2) A_3^n(t)}{(\lambda_3-\lambda_1)(\lambda_3-\lambda_2)} \right\} \\ \left. - (1-F) k_l \left(\displaystyle\sum_{n=1,odd}^{\infty} \dfrac{8}{\pi^2} \dfrac{1}{k_l\tau - n^2} \right) \left[\dfrac{(\lambda_2+\lambda_3) B_1(t)}{(\lambda_1-\lambda_2)(\lambda_1-\lambda_3)} + \dfrac{(\lambda_1+\lambda_3) B_2(t)}{(\lambda_2-\lambda_1)(\lambda_2-\lambda_3)} + \dfrac{(\lambda_1+\lambda_2) B_3(t)}{(\lambda_3-\lambda_1)(\lambda_3-\lambda_2)} \right] \right) \\ I_2(t) = A_{\text{surf}} a \left\{ \dfrac{F}{\tau} \dfrac{8}{\pi^2} \displaystyle\sum_{n=1,odd}^{\infty} \left[\dfrac{A_1^n(t)}{(\lambda_1-\lambda_2)(\lambda_1-\lambda_3)} + \dfrac{A_2^n(t)}{(\lambda_2-\lambda_1)(\lambda_2-\lambda_3)} + \dfrac{A_3^n(t)}{(\lambda_3-\lambda_1)(\lambda_3-\lambda_2)} \right] \right. \\ + (1-F) k_l \displaystyle\sum_{n=1,odd}^{\infty} \dfrac{8}{\pi^2} \dfrac{1}{k_l\tau - n^2} \left\{ \dfrac{A_1^n(t)}{(\lambda_1-\lambda_2)(\lambda_1-\lambda_3)} + \dfrac{A_2^n(t)}{(\lambda_2-\lambda_1)(\lambda_2-\lambda_3)} + \dfrac{A_3^n(t)}{(\lambda_3-\lambda_1)(\lambda_3-\lambda_2)} \right\} \\ \left. - (1-F) k_l \left(\displaystyle\sum_{n=1,odd}^{\infty} \dfrac{8}{\pi^2} \dfrac{1}{k_l\tau - n^2} \right) \left[\dfrac{B_1(t)}{(\lambda_1-\lambda_2)(\lambda_1-\lambda_3)} + \dfrac{B_2(t)}{(\lambda_2-\lambda_1)(\lambda_2-\lambda_3)} + \dfrac{B_3(t)}{(\lambda_3-\lambda_1)(\lambda_3-\lambda_2)} \right] \right) \end{array} , \quad (25)$$

where $A_i^n(t)$ and $B_i(t)$ are given in Equation (17b).

The MATLAB [22] codes that use the above equations to plot the solutions for the SM and the SMK models are provided as Supplementary Material files.

2.3. Having a Time-Dependent **A** *Matrix*

Before closing this work, it may appear to the reader that, given the complete analytical solution for $M_l(t)$, there may be an explicit analytical solution to PBTK (and PBPK) models in which the kinetic rates are arbitrary time-dependent functions. Having time-dependent kinetic rates in PBTK models is necessary to accurately predict *in vivo* implantation data in mice [3]. Although this is in general true, certain conditions must be met. In particular, such a solution can be sought only when $\mathbf{A}(t)$ commutes with its integral [23], i.e.,

$$\mathbf{A}(t) \cdot \left[\int_0^t \mathbf{A}(x)dx \right] = \left[\int_0^t \mathbf{A}(x)dx \right] \cdot \mathbf{A}(t), \quad (26)$$

As an example, for the SM model, the following should hold:

$$\begin{bmatrix} \{k_{st}(t)+k_u(t)\}\int_0^t\{k_{st}(x)+k_u(x)\}dx+k_{ts}(t)\int_0^t k_{st}(x)dx & -\{k_{st}(t)+k_u(t)\}\int_0^t k_{ts}(x)dx-k_{ts}(t)\int_0^t k_{ts}(x)dx \\ -k_{st}(t)\int_0^t\{k_{st}(x)+k_u(x)\}dx-k_{ts}(t)\int_0^t k_{st}(x)dx & k_{st}(t)\int_0^t k_{ts}(x)dx+k_{ts}(t)\int_0^t k_{ts}(x)dx \end{bmatrix} = \begin{bmatrix} \{k_{st}(t)+k_u(t)\}\int_0^t\{k_{st}(x)+k_u(x)\}dx+k_{st}(t)\int_0^t k_{st}(x)dx & -k_{ts}(t)\int_0^t(k_{st}(x)+k_u(x))dx-k_{ts}(t)\int_0^t k_{ts}(x)dx \\ -\{k_{st}(t)+k_u(t)\}\int_0^t k_{st}(x)dx-k_{ts}(t)\int_0^t k_{ts}(x)dx & k_{ts}(t)\int_0^t k_{st}(x)dx+k_{ts}(t)\int_0^t k_{ts}(x)dx \end{bmatrix}, \quad (27)$$

meaning that

$$\begin{aligned} k_{ts}(t)\int_0^t k_{st}(x)dx &= k_{st}(t)\int_0^t k_{ts}(x)dx \\ k_u(t)\int_0^t k_{ts}(x)dx &= k_{ts}(t)\int_0^t k_u(x)dx \\ k_u(t)\int_0^t k_{st}(x)dx &= k_{st}(t)\int_0^t k_u(x)dx \end{aligned} \quad (28)$$

Note that by taking the ratio between the last two equations, we end up with the first equation. Thus, only two of the equations must be met. In general, these conditions are not met, and thus, a general solution with a time-dependent **A** matrix is not possible. Additional requirements may need to be held for more complicated PBTK or PBPK models.

3. Results and Discussion

The results presented here are based on the kinetic parameters derived from a model parameterization procedure outlined in our previous study [2]. In that procedure, we considered a time-variant simplified version of the SM model, named SSM, which assumes that the tissue-serum exchange rates are much faster than in all the remaining compartments. Additionally, we utilized the SMK model along with Equation (15), incorporating the *in vitro* results obtained from the compressed oxidized tube (OT) stents, as reported by [24]. However, since the analytical solutions are based on time-invariant ODEs and the SM model instead of the SSM, the parameterization procedure was repeated in this work with time-independent kinetic rates. The results of the parameterization are summarized in Table 1. The readers are here reminded that both SM and SMK models' predictive capacity has been validated against reported values following implantation of atrium occluders in humans [17] and stent implantation in minipigs [13] by Giakoumi et al. [2].

Table 1. Parameters and constants that were used in the calculations presented in Section 3.

Parameter/Model	SM	SMK
F	0.56	0.56
$k_l(1/\text{day})$	0.0582	0.118
$k_{ts}(1/\text{day})$	0.996	0.595
$k_{st}(1/\text{day})$	22.0	11.91
$k_{ks}(1/\text{day})$	-	9.94
$k_{sk}(1/\text{day})$	-	13.89
$k_u(1/\text{day})$	1.18	0.92
$k_g(1/\text{day})$	1.38	1.38
$a(\mu\text{g}/\text{cm}^2)$	11.697	11.697

Table 1. *Cont.*

Parameter/Model	SM	SMK
τ(days)	15.215	15.215
$A_{\text{surf}}(\text{cm}^2)$	33.7	33.7
V_s(L)	2.55	2.55
Q_u(L/day)	4	4

3.1. Speed of Computations

In Table 2, we report the computation time needed when the calculations are executed using the analytical solutions provided in the previous section and compare it with the one needed when the computations are executed using ODE numerical solvers (using ode45 ODE solver of MATLAB). The truncation of the infinite series when using Equation (15) was determined based on a tolerance criterion. Specifically, the series was truncated when the next term to be added was less than 10^{-5}; for the release parameters of the OT stent, this criterion resulted in considering 285 terms. We note that the analytical solution is faster for both the SM and SMK models, irrespective of the expression employed for $M_d(t)$; however, the more complicated the model [SMK vs. SM and single exponential, Equation (S1), vs. multiple exponential device release, Equation (15)], the relative speed decreases.

Table 2. ODE numerical solver (ode45 of MATLAB) versus analytical solutions: comparison of computation time (in seconds).

	Analytical Solution	Numerical Solution	Ratio (Numerical/Analytical Solution)
SM—Equation (S1)	0.0001504	0.02336	157.05518
SM—Equation (15)	0.0190181	0.0466662	2.453778
SMK—Equation (S1)	0.0001949	0.0315174	161.710620
SMK—Equation (15)	0.0360561	0.1031546	2.860947

3.2. Model Predictions

We depict in Figure 1 the predictions of the SM model, Equations (14) and (17), as provided by its analytical solutions when we consider the infinite-exponential device release, Equation (15). In Figure 1a we depict the solution for the Ni mass accumulation in the local tissue as given by Equation (16). We note that by increasing the parameters F and the kinetic rate k_l the mass accumulated decreases; this is expected as by increasing F less Ni is released into the local tissue, and by increasing k_l, the Ni mass exchange rate from the local tissue to serum increases; in addition, by increasing k_l the position of the maximum is noted to shift to smaller times. Then, in Figure 1b,c we depict the Ni concentration profiles in the serum, C_s, and urine, C_u, compartments, respectively, for various model parameters. As expected, we note the reverse behavior relative to the local tissue predictions, since as F and k_l increase the Ni mass accumulation in serum is noted to increase and the position of the maximum is again noted to shift to smaller times; the same trend is noted when increasing the parameter k_{ts} since it controls the Ni mass exchange rate from the other tissues compartment to serum, whereas the reverse occurs by increasing the parameter k_{st} that controls the reverse exchange. The behavior in the urine compartment is similar to the one noted in the serum compartment since C_u is simply proportional to C_s via Equation (4b). Finally, in Figure 1d we depict the Ni concentration profiles in the other tissues compartment, where we note a similar behavior as in the serum compartment when keeping k_{st} and k_{ts} constant: by increasing F and k_l the curves shift upwards; however, when the k_{ts} is increased the Ni mass accumulation decreases since this kinetic rate controls the Ni mass exchange rate from the other tissues compartment to serum. The reverse

occurs by increasing the k_{st} parameter; both behaviors are what we would expect. Next, we depict in Figure 2 the predictions of the SMK model as provided by its analytical solutions, Equations (24) and (25), when we consider the infinite-exponential device release, Equation (15). Note that the local tissue compartment predictions are not offered as they are the same as the ones obtained using the SM model [Figure 1a], see Equation (16). In the left column, we depict the predictions while keeping the values of k_{ks} and k_{sk} fixed, whereas in the right column, we depict the predictions while keeping the values of F and k_l fixed. The predictions for the serum and urine compartments [Figure 2a,b] are similar to the ones obtained when using the SM model; the predictions for the kidney compartment [Figure 2c] are also similar to the serum and urine compartments. We should here note that in the SMK model, C_s is proportional to M_k and not C_s via the last equation of Equation (18a). Finally, the predictions for the other tissue compartment [Figure 2d] are similar to the ones obtained when using the SM model. Finally, we note that by increasing the kinetic rate k_{ks} the mass accumulated in the serum and other tissue compartments [Figure 2e,h] increases, whereas the accumulation in the kidney and urine compartments [Figure 2f,g] decreases, an expected outcome since this kinetic rate controls the Ni mass exchange rate from kidneys to serum. The reverse behavior in these compartments is noted when the kinetic rate k_{sk} increases.

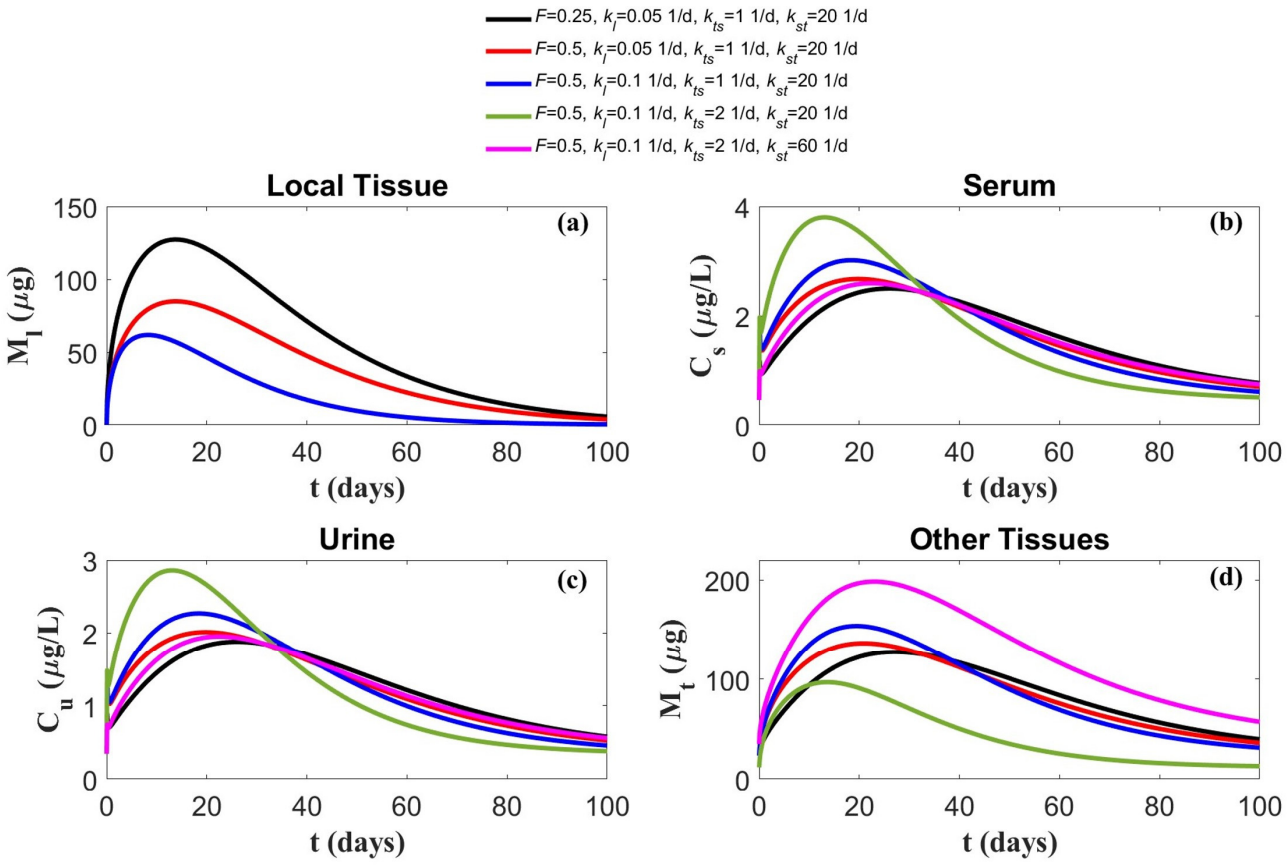

Figure 1. SM model derived-predictions of the nickel concentration–time profiles in the tissue and body fluid compartments for varying values of the model parameters. The parameters k_u, k_g, A_{surf}, a, τ, V_s, Q_u are kept constant and equal to the values provided in Table 1. Note that the local tissue profile only depends on F and k_l.

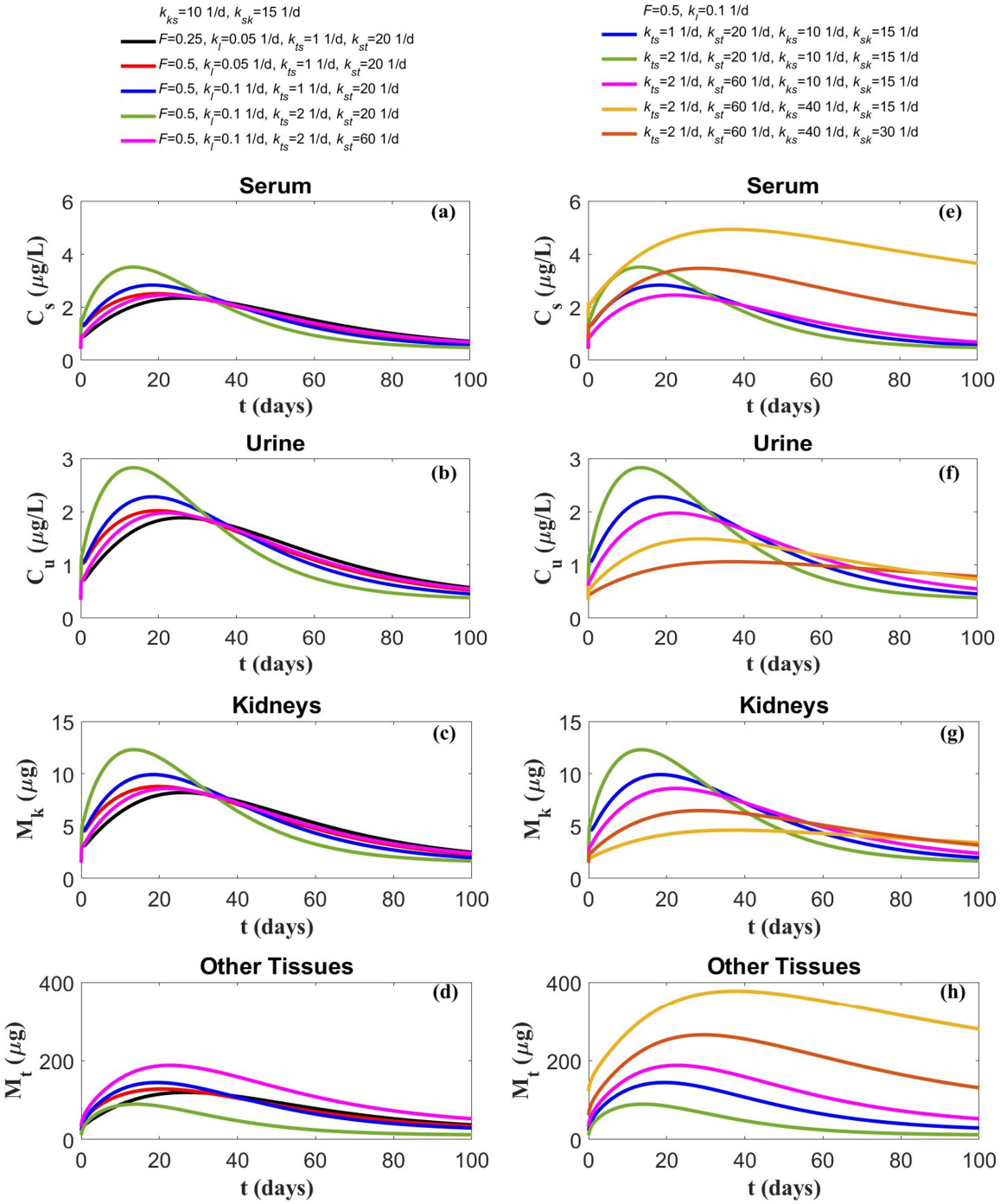

Figure 2. SMK model derived predictions of the nickel concentration–time profiles in the tissue and body fluid compartments for varying values of the model parameters. The parameters k_u, k_g, A_{surf}, a, τ, V_s, Q_u are kept constant and equal to the values provided in Table 1.

This difference can be explained by the additional terms in the series presented in Equation (15) that include a spectrum of characteristic times smaller than τ, which offset the leaching rate at earlier times, leading to an earlier attainment of the maximum values.

While Equation (S1) [and in turn Equations (S5a) and (S5b)] and Equation (15) offer valuable predictions, being dependent solely on the parameters a, τ and k_l, might be too simplistic for real biological systems, where multiple interacting factors influence these values. A recent U.S. FDA review [25], based on experimental and clinical data, collectively reported that metal implants experience different degrees of wear and corrosion due to

the mechanical and biochemical environment at the specific site of implantation that can ultimately affect the ion diffusion profile and kinetics. These findings emphasize the significance of taking into account the implantation site when designing testing setups or *in silico* models to predict the leaching profile of implant byproducts and underscore the importance of the biomechanochemical environment at the device−tissue interface.

3.3. Model Applications

One of the most important outcomes of PBTK modeling is the ability to predict the biodistribution of toxic substances or implant byproducts. This type of testing allows the estimation of exposure as part of toxicological risk assessment per ISO 10993 [26] and facilitates easy comparison between devices, providing a framework for comparing different alloys, designs, or manufacturing processes [which would impact the parameters a and τ in Equation (S1) and Equation (15)]. The PBTK model-derived outputs are employed here to predict the leaching profile of nickel (i.e., the maximum nickel mass value and the time required to reach this maximum in the various tissue and body fluid compartments) and its dependency on the surface diffusion parameters. The acquired data can be utilized to assess whether Ni exposure levels exceed permissible limits and determine the toxicological safety of implants with different designs and physicochemical characteristics. As we focus on human exposure, we concentrate on the values of the model parameters (using both the SM and SMK models) reported in Table 1.

We should stress that while a single-exponential, Equation (S1), or infinite-exponential, Equation (15), surface diffusion profile conforms to the classical passive diffusion of Ni and aligns with the experimental findings of Sullivan et al. [24] and others [3,27–29], it is crucial to acknowledge that these equations do not provide a comprehensive description of all reported substance-release expressions in the existing literature. As one example, we mention the latest work by Saylor et al. [30] in which release rates are reported to be proportional to $t^{3/4}$ and $t^{1/4}$ for different surface finishes of NiTi, which deviate from the $t^{1/2}$ behavior predicted by both Equation (S1) and Equation (15) at small time scales. Notably, these observations suggest that the complete depletion of Ni may take several years to decades. This contrasts the behavior of the devices reported in Figure S1 of our previous work [2], where the single-exponential and infinite-exponential expressions have been used, showing a complete depletion after 2–3 months. In addition, many implants, especially cardiovascular ones, are subjected to a dynamic biomechanical *in vivo* environment, which may increase ion release into surrounding tissues. This complex leaching behavior [31] cannot be adequately captured using a single or infinite-exponential diffusion profile but most probably requires considering the additional stress-induced diffusion [32] when medical devices are under constant bending and the fluid dynamical conditions which would increase the mass transfer coefficient that should depend on the Reynolds number for laminar flows [33] or the Womersley number for pulsatile flows. We should also recall here that due to device endothelialization, almost all ion mass leached from the device is eventually taken up by the local tissue compartment, which occurs theoretically after approximately 7–28 days, as reported in animal models [34,35] and the clinic [36]. Similar deviations between expected experimental results and the theoretical predictions proposed by Equation (S1) and Equation (15) could also occur for other substances released from implantable medical devices.

We depict the maximum value of the Ni accumulation using the more realistic multiple-exponential device release expression, Equation (15) in the local tissue in Figure 3 (common for both the SM and SMK models), and in the serum, urine, and other tissues compartments for the SM model in Figures 4–6, respectively. We find that all of them exhibit the same behavior: the smaller the values of a and τ are, the smaller the maximum value of Ni in all compartments is. Of the two parameters, a seems to be the most influential on the maximum mass value, whereas the time required to reach this maximum is solely impacted by the τ parameter. Similar behavior is also noted for the maximum value of the Ni accumulation and the time it occurs in the serum, urine, other tissues, and kidney compartments for the SMK

model depicted in Figures 7–10, respectively. We also mark that the SMK model predicts a higher maximum mass value and a shorter time at which it occurs relative to the SM model for the serum, and urine compartments. This is most probably due to the higher flexibility demonstrated by the five-compartment SMK model. In comparing the two device release expressions [Equation (S1) vs. Equation (15)] for determining the maximum values of Ni accumulation in all compartments [cf. Figures 3–10 with Figures S1–S8], it is observed that there is a negligible change in the accumulation values. However, there is a decrease in the time at which the maximum value is reached in the case of Equation (S1).

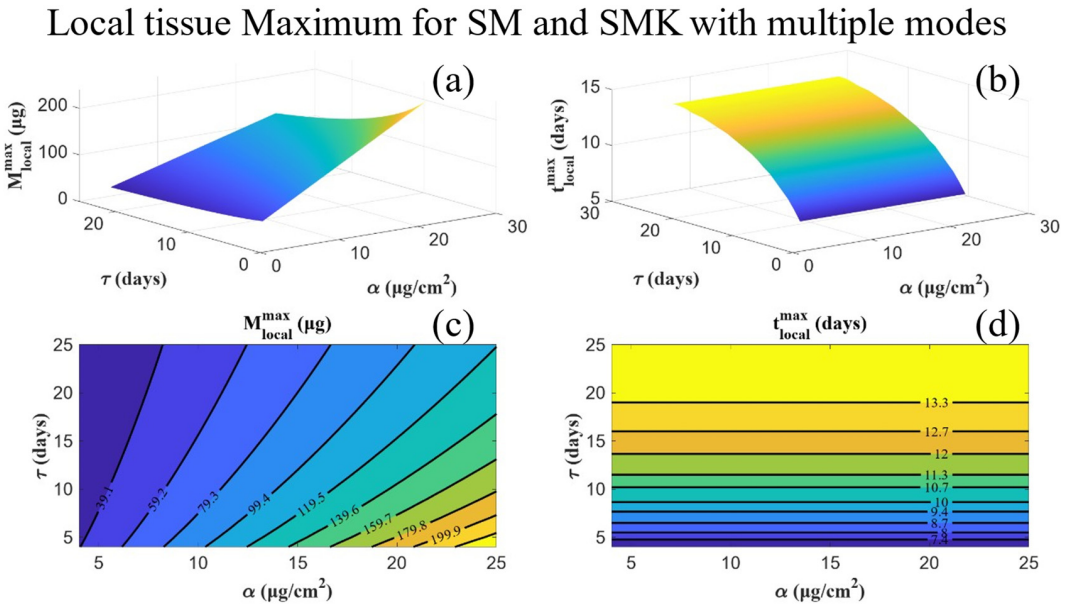

Figure 3. (**a**) The maximum Ni mass value and (**b**) the time it occurs in the local tissue compartment for both the SM and SMK model when using Equation (15). The corresponding contour plots are also depicted in parts (**c**) and (**d**), respectively.

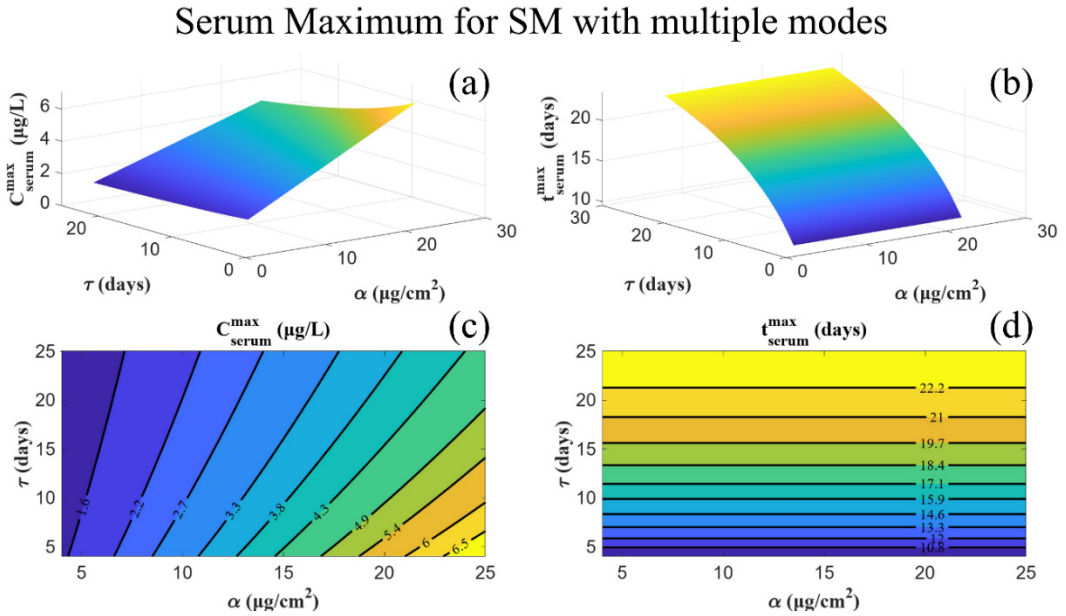

Figure 4. (**a**) The maximum Ni mass value and (**b**) the time it occurs in the serum compartment for the SM model when using Equation (15). The corresponding contour plots are also depicted in parts (**c**) and (**d**), respectively.

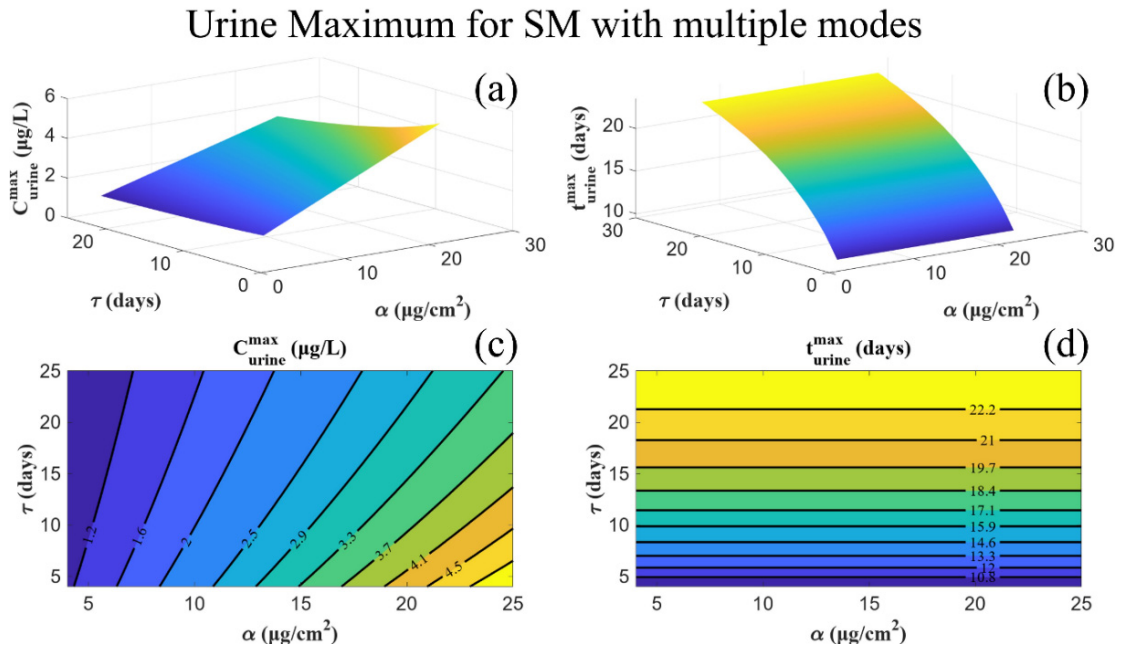

Figure 5. (**a**) The maximum Ni mass value and (**b**) the time it occurs in the urine compartment for the SM model when using Equation (15). The corresponding contour plots are also depicted in parts (**c**) and (**d**), respectively.

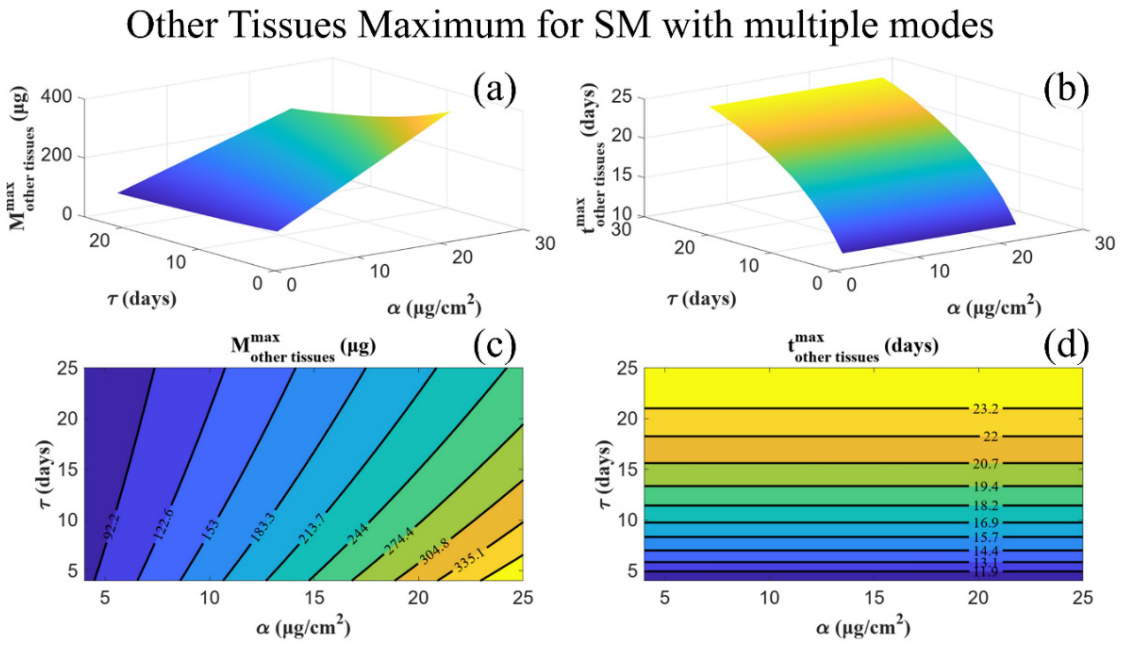

Figure 6. (**a**) The maximum Ni mass value and (**b**) the time it occurs in the other tissues compartment for the SM model when using Equation (15). The corresponding contour plots are also depicted in parts (**c**) and (**d**), respectively.

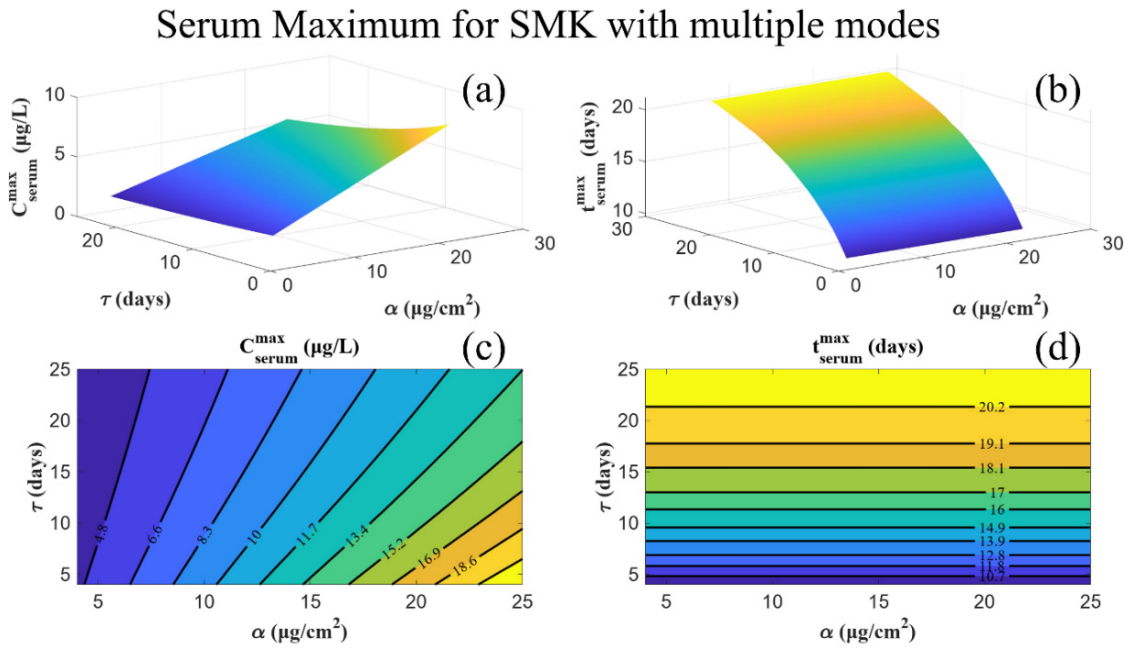

Figure 7. (**a**) The maximum Ni mass value and (**b**) the time it occurs in the serum compartment for the SMK model when using Equation (15). The corresponding contour plots are also depicted in parts (**c**) and (**d**), respectively.

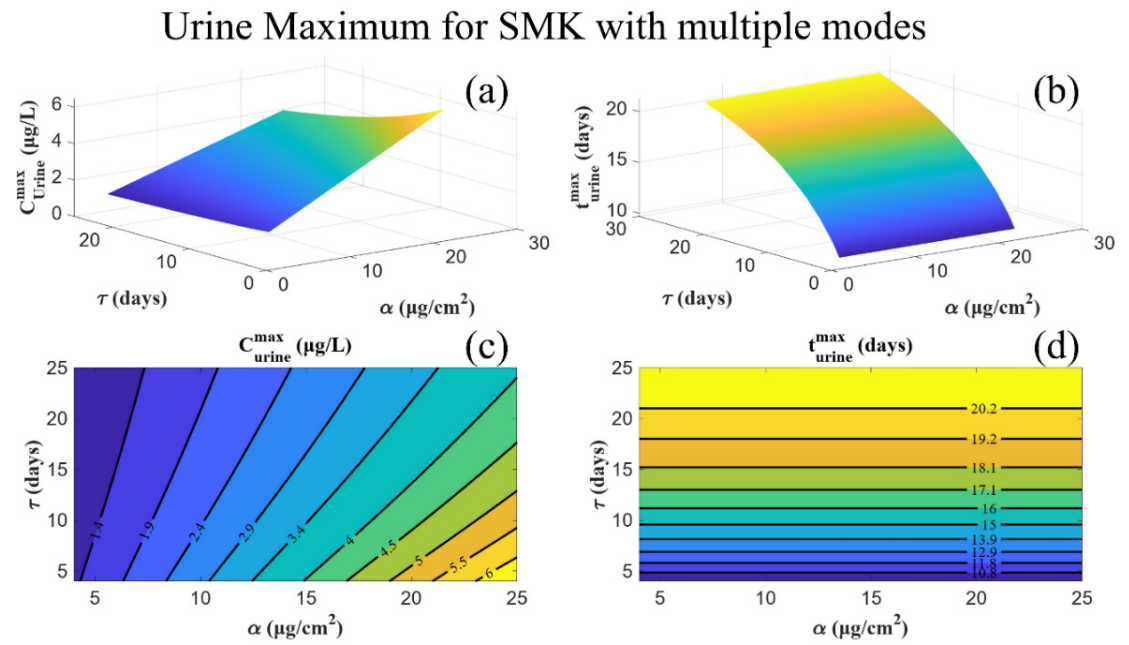

Figure 8. (**a**) The maximum Ni mass value and (**b**) the time it occurs in the urine compartment for the SMK model when using Equation (15). The corresponding contour plots are also depicted in parts (**c**) and (**d**), respectively.

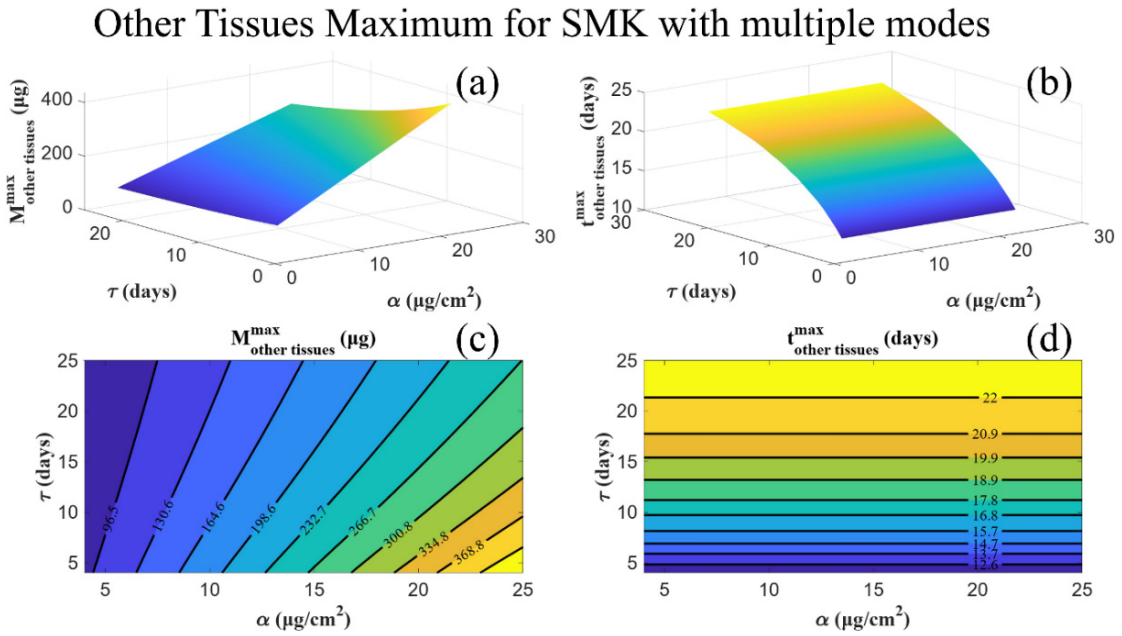

Figure 9. (**a**) The maximum Ni mass value and (**b**) the time it occurs in the other tissues compartment for the SMK model when using Equation (15). The corresponding contour plots are also depicted in parts (**c**) and (**d**), respectively.

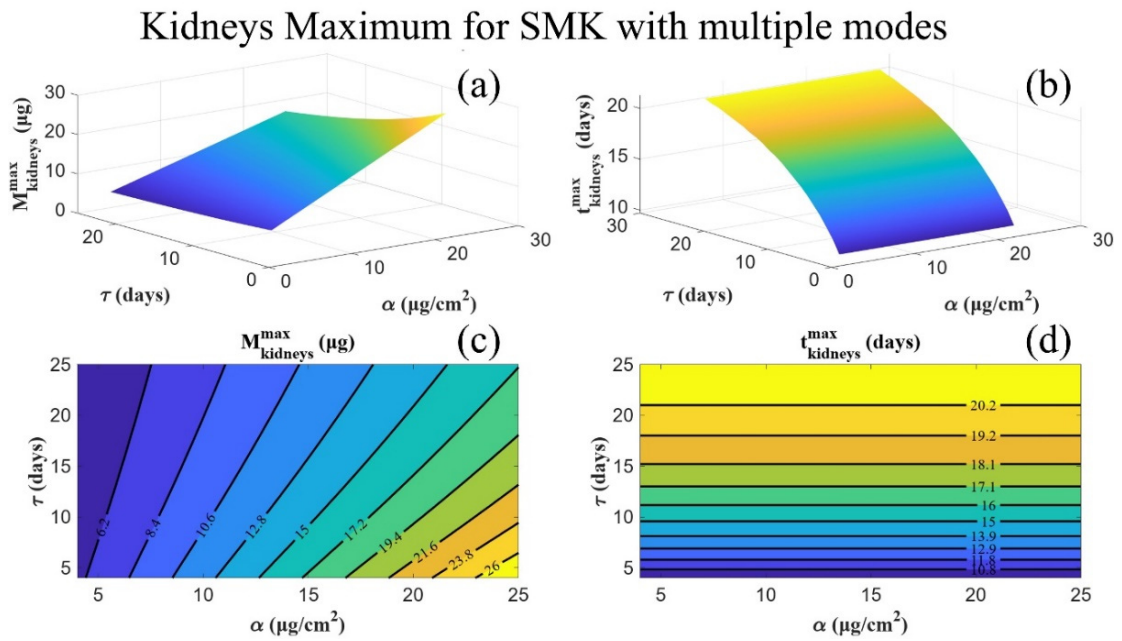

Figure 10. (**a**) The maximum Ni mass value and (**b**) the time it occurs in the kidneys compartment for the SMK model when using Equation (15). The corresponding contour plots are also depicted in parts (**c**) and (**d**), respectively.

4. Conclusions

The main purpose of this paper was to derive analytical solutions for PBTK models that, to the best of our knowledge, are a first in the literature. The use of computational modeling and simulation in regulatory submissions is rapidly increasing since PBTK models can estimate the inferred *in vivo* exposure based only on the results of *in vitro* testing. The FDA promotes and facilitates the use of nonanimal methods in testing and research [7,37]; hence, PBTK and PBPK models will soon become a prerequisite for evaluating the toxi-

cological safety and effectiveness of medical devices and pharmaceuticals, respectively, prioritizing the availability of analytical solutions. We have shown that analytical solving bears speed advantages over solutions obtained using ODE numerical solvers. This is of great importance in promoting the use of *in silico* models, especially when the solver needs to be coupled with a real-time interface for web-based apps [14]. Furthermore, analytical solutions are accurate and easier to use in optimization procedures for model parameterization. In contrast, numerical solutions of ODEs, especially for stiff problems, often yield non-smooth objective functions, making gradient-based methods ineffective and requiring more computationally demanding algorithms. In all cases, our analysis indicates that the maximum mass value in all compartments is predominantly influenced by the amount of surface-connected nickel per device surface area whereas the time required to reach this maximum is solely impacted by the characteristic release time. This type of information is instrumental to medical device manufacturers aiming to optimize surface characteristics and processing methods to minimize ion leaching and comply with permissible exposure limits.

Supplementary Materials: The following supporting information can be downloaded at: https://www.mdpi.com/article/10.3390/mca29060101/s1. The MATLAB codes that use the analytical solutions and plot them and a supplementary document are provided as supplementary material.

Author Contributions: M.G.: methodology, software, validation, formal analysis, investigations, data curation, writing—review and editing, visualization; K.K.: conceptualization, methodology, formal analysis, writing—review and editing, supervision, project administration; A.A.: writing—review and editing; P.S.S.: conceptualization, methodology, software, validation, formal analysis, investigations, writing—review and editing, supervision, project administration. All authors have read and agreed to the published version of the manuscript.

Funding: No funding was received for conducting this study.

Data Availability Statement: The data presented in the study are included in the article, and the MATLAB codes to plot the analytical solutions are available as Supplementary Materials. Further inquiries can be directed to the corresponding author.

Conflicts of Interest: The authors confirm that they have given due consideration to the protection of intellectual property associated with this work (PCT/EP2022/064468 and US 2024/0249808 A1) and that there are no impediments to publication, including the timing of publication, with respect to intellectual property. In so doing, the authors confirm that they have followed the regulations of their institution concerning intellectual property. The authors also declare that they have no known competing financial interests or personal relationships that could have appeared to influence the work reported in this paper.

References

1. Chen, M.; Du, R.; Zhang, T.; Li, C.; Bao, W.; Xin, F.; Hou, S.; Yang, Q.; Chen, L.; Wang, Q.; et al. The Application of a Physiologically Based Toxicokinetic Model in Health Risk Assessment. *Toxics* **2023**, *11*, 874. [CrossRef] [PubMed]
2. Giakoumi, M.; Stephanou, P.S.; Kapnisis, K.; Anayiotos, A. On the Development of Physiologically Based Toxicokinetic (PBTK) Models for Cardiovascular Implants. *Regul. Toxicol. Pharmacol.* **2023**, *144*, 105489. [CrossRef] [PubMed]
3. Giakoumi, M.; Stephanou, P.S.; Kokkinidou, D.; Papastefanou, C.; Anayiotos, A.; Kapnisis, K. A Predictive Toxicokinetic Model for Nickel Leaching from Vascular Stents. *ACS Biomater. Sci. Eng.* **2024**, *10*, 2534–2551. [CrossRef] [PubMed]
4. Mielke, H.; Gundert-Remy, U. Physiologically Based Toxicokinetic Modelling as a Tool to Support Risk Assessment: Three Case Studies. *J. Toxicol.* **2012**, *2012*, 359471. [CrossRef]
5. Moradi Kashkooli, F.; Soltani, M.; Souri, M.; Meaney, C.; Kohandel, M. Nexus between in Silico and in Vivo Models to Enhance Clinical Translation of Nanomedicine. *Nano Today* **2021**, *36*, 101057. [CrossRef]
6. Siepmann, J.; Siepmann, F. Mathematical Modeling of Drug Delivery. *Int. J. Pharm.* **2008**, *364*, 328–343. [CrossRef] [PubMed]
7. U.S. Food and Drug Administration. Assessing the Credibility of Computational Modeling and Simulation in Medical Device Submissions. Available online: https://www.fda.gov/regulatory-information/search-fda-guidance-documents/assessing-credibility-computational-modeling-and-simulation-medical-device-submissions (accessed on 12 September 2024).
8. VPH Institute. In Silico Medicine Is Now in the ECDC Regulation! Available online: https://www.vph-institute.org/news/in-silico-medicine-is-now-in-the-ecdc-regulation.html (accessed on 12 September 2024).

9. Parthasarathi, R.; Dhawan, A. In Silico Approaches for Predictive Toxicology. In *In Vitro Toxicology*; Academic Press: Cambridge, MA, USA, 2018; pp. 91–109, ISBN 9780128047712.
10. Krishnan, K.; Peyret, T. Physiologically Based Toxicokinetic (PBTK) Modeling in Ecotoxicology. In *Ecotoxicology Modeling, Emerging Topics in Ecotoxicology: Principles, Approaches and Perspectives 2*; Springer: Boston, MA, USA, 2009; pp. 145–175, ISBN 978-1-4419-0197-2.
11. Fisher, J.W.; Gearhart, J.M.; Lin, Z. *Physiologically Based Pharmacokinetic (PBPK) Modeling: Methods and Applications in Toxicology and Risk Assessment*; Academic Press: Cambridge, MA, USA, 2020.
12. Saylor, D.M.; Adidharma, L.; Fisher, J.W.; Brown, R.P. A Biokinetic Model for Nickel Released from Cardiovascular Devices. *Regul. Toxicol. Pharmacol.* **2016**, *80*, 1–8. [CrossRef]
13. Nagaraja, S.; Sullivan, S.J.L.; Stafford, P.R.; Lucas, A.D.; Malkin, E. Impact of Nitinol Stent Surface Processing on In-Vivo Nickel Release and Biological Response. *Acta Biomater.* **2018**, *72*, 424–433. [CrossRef]
14. Abuhelwa, A.Y.; Foster, D.J.R.; Upton, R.N. ADVAN-Style Analytical Solutions for Common Pharmacokinetic Models. *J. Pharmacol. Toxicol. Methods* **2015**, *73*, 42–48. [CrossRef]
15. Dorf, R.C.; Bishop, R.H. *Modern Control Systems, Global Edition*; Pearson Education Limited: London, UK, 2017; ISBN 978-1-292-15297-4.
16. Meyer, C.D. *Matrix Analysis and Linear Algebra*; Society for Industrial & Applied Mathematics: Philadelphia, PA, USA, 2000; ISBN 0898714540.
17. Burian, M.; Neumann, T.; Weber, M.; Brandt, R.; Geisslinger, G.; Mitrovic, V.; Hamm, C. Nickel Release, a Possible Indicator for the Duration of Antiplatelet Treatment, from a Nickel Cardiac Device in Vivo: A Study in Patients with Atrial Septal Defects Implanted with an Amplatzer Occluder. *Int. J. Clin. Pharmacol. Ther.* **2006**, *44*, 107–112. [CrossRef]
18. Tzafriri, A.R.; Groothuis, A.; Price, G.S.; Edelman, E.R. Stent Elution Rate Determines Drug Deposition and Receptor-Mediated Effects. *J. Control Release* **2012**, *161*, 918–926. [CrossRef] [PubMed]
19. Barocas, V.; William, D.; Girton, T.; Guler, I.; Knapp, D.; Moeller, J.; Parsonage, E. A Dissolution-Diffusion Model for the TAXUS^{TM} Drug-Eluting Stent with Surface Burst Estimated from Continuum Percolation. *J. Biomed. Mater. Res. Part B Appl. Biomater.* **2009**, *90*, 267–274. [CrossRef] [PubMed]
20. Higuchi, T. Rate of Release of Medicaments from Ointment Bases Containing Drugs in Suspension. *J. Pharm. Sci.* **1961**, *50*, 874–875. [CrossRef] [PubMed]
21. Verriest, E.I.; Hyun, N.P. Roots of Polynomials with Positive Coefficient. In Proceedings of the 3rd International Symposium on Mathematical Theory of Networks and Systems, Hong Kong, China, 16–20 July 2018.
22. The MathWorks Inc. *MATLAB, R2023b*; MathWorks Inc.: Natick, MA, USA, 2023.
23. Martin, J.F.P. On the Exponential Representation of Solutions of Linear Differential Equations. *J. Differ. Equ.* **1968**, *4*, 257–279. [CrossRef]
24. Sullivan, S.J.L.; Dreher, M.L.; Zheng, J.; Chen, L.; Madamba, D.; Miyashiro, K.; Trépanier, C.; Nagaraja, S. Effects of Oxide Layer Composition and Radial Compression on Nickel Release in Nitinol Stents. *Shape Mem. Superelasticity* **2015**, *1*, 319–327. [CrossRef]
25. U.S. Food and Drug Administration. *Biological Responses to Metal Implants*; U.S. Food and Drug Administration: Silver Spring, MD, USA, 2019.
26. U.S. Food and Drug Administration. *Use of International Standard ISO 10993-1, "Biological Evaluation of Medical Devices—Part 1: Evaluation and Testing Within a Risk Management Process"*; U.S. Food and Drug Administration: Silver Spring, MD, USA, 2023.
27. Nagaraja, S.; Sena, G.; Stafford, P.; Braeuner, C.; Hempel, P.; Pelton, A.R.; Ravi, V. Effects of Nitinol Microstructural Purity on Localized and Uniform Corrosion Susceptibility. *Shape Mem. Superelast.* **2022**, *8*, 118–128. [CrossRef]
28. Nagaraja, S.; Pelton, A.R. Corrosion Resistance of a Nitinol Ocular Microstent: Implications on Biocompatibility. *J. Biomed. Mater. Res. Part B Appl. Biomater.* **2020**, *108*, 2681–2690. [CrossRef]
29. Sussman, E.M.; Shi, H.; Turner, P.A.; Saylor, D.M.; Weaver, J.D.; Simon, D.D.; Takmakov, P.; Sivan, S.; Shin, H.Y.; Di Prima, M.A.; et al. Nitinol Release of Nickel under Physiological Conditions: Effects of Surface Oxide, PH, Hydrogen Peroxide, and Sodium Hypochlorite. *Shape Mem. Superelast.* **2022**, *8*, 98–106. [CrossRef]
30. Saylor, D.M.; Sivan, S.; Turner, P.; Shi, H.; Soneson, J.E.; Weaver, J.D.; Di Prima, M.; Sussman, E.M. Temperature Dependence of Nickel Ion Release from Nitinol Medical Devices. *J. Biomed. Mater. Res. Part B Appl. Biomater.* **2021**, *109*, 1188–1197. [CrossRef]
31. Nagaraja, S.; Chandrasekar, V.; Ormonde, D.; Hickey, H.; Lipschultz, K.; Chao, C.; Vilendrer, K.; Pelton, A.R. The Impact of Fatigue Testing and Surface Processing on Nickel Release in Nitinol Stents. *Shape Mem. Superelast.* **2018**, *4*, 462–471. [CrossRef]
32. Frolova, K.P.; Vilchevskaya, E.N.; Bessonov, N.M. On Modeling of Stress-Induced Diffusion within Micropolar and Classical Approaches. *ZAMM—J. Appl. Math. Mech./Z. Angew. Math. Mech.* **2022**, *102*, e202100505. [CrossRef]
33. Abrahamsson, B.; Pal, A.; Sjöberg, M.; Carlsson, M.; Laurell, E.; Brasseur, J.G. A Novel in Vitro and Numerical Analysis of Shear-Induced Drug Release from Extended-Release Tablets in the Fed Stomach. *Pharm. Res.* **2005**, *22*, 1215–1226. [CrossRef] [PubMed]
34. de Prado, A.P.; Pérez-Martínez, C.; Cuellas-Ramón, C.; Gonzalo-Orden, J.M.; Regueiro-Purriños, M.; Martínez, B.; García-Iglesias, M.J.; Ajenjo, J.M.; Altónaga, J.R.; Diego-Nieto, A.; et al. Time Course of Reendothelialization of Stents in a Normal Coronary Swine Model: Characterization and Quantification. *Vet. Pathol.* **2011**, *48*, 1109–1117. [CrossRef] [PubMed]
35. Zhang, B.; Zheng, B.; Wang, X.; Shi, Q.; Jia, J.; Huo, Y.; Pan, C.; Han, J.; Chen, M. Polymer-Free Dual Drug-Eluting Stents Evaluated in a Porcine Model. *BMC Cardiovasc. Disord.* **2017**, *17*, 222. [CrossRef]

36. Cornelissen, A.; Vogt, F.J. The Effects of Stenting on Coronary Endothelium from a Molecular Biological View: Time for Improvement? *J. Cell. Mol. Med.* **2019**, *23*, 39–46. [CrossRef]
37. U.S. Food and Drug Administration. *Technical Considerations for Non-Clinical Assessment of Medical Devices Containing Nitinol*; U.S. Food and Drug Administration: Silver Spring, MD, USA, 2021.

Disclaimer/Publisher's Note: The statements, opinions and data contained in all publications are solely those of the individual author(s) and contributor(s) and not of MDPI and/or the editor(s). MDPI and/or the editor(s) disclaim responsibility for any injury to people or property resulting from any ideas, methods, instructions or products referred to in the content.